

RESEARCH ARTICLE OPEN ACCESS

Poly(propylene glycol) Diacrylate Crosslinker in Gel Polymer Electrolytes for Glass-based Electrochromic Devices

 Selma Dahms  | Lukas Niklaus  | Marco Schott 

Fraunhofer Institute for Silicate Research ISC, Würzburg, Germany

Correspondence: Marco Schott (marco.schott@isc.fraunhofer.de)

Received: 3 November 2025 | **Revised:** 16 December 2025 | **Accepted:** 19 December 2025

Keywords: acrylate crosslinker | cycling stability | electrochromic devices | gel polymer electrolyte | response time

ABSTRACT

Electrochromic devices (ECDs) are promising as smart windows, as they provide dynamic control over light transmission and contribute to reducing energy costs in buildings. However, sluggish response times and low cycling stability highlight key barriers to their commercialization. One approach to tackle these is to optimize gel polymer electrolytes (GPEs) for ECDs, as they already balance high ionic conductivity and low risk of leakage. This study compares the GPE compositions with and without crosslinker poly(propylene glycol) diacrylate (PPGDA) in hybrid and inorganic ECDs. These include Fe(II) metal coordination polymer (Fe(II)-MCP) with Prussian blue (PB) and WO_3 with NiO_x . Some of the ECD performance parameters are not altered, like contrast ratio and coloration efficiencies, as they correspond to the electrochromic materials. By adding PPGDA to the GPE the charge density is lower for both cell types and the cyclability over 1000 switching cycles is demonstrated. Additionally, PPGDA reduces the bleaching time for the WO_3/NiO_x device, while the coloring time of the Fe(II)-MCP/PB devices slightly increases. These results show the benefits of the crosslinker PPGDA in a GPE on response time and cycling stability of two various ECDs.

1 | Introduction

The global need for sustainable heat and advanced light control in buildings drives the rising demand for energy-efficient electrochromic (EC) windows [1, 2]. Accordingly, the optimization of EC windows represents a critical pathway toward reducing energy costs and advancing carbon neutrality goals [3]. In general, EC devices (ECDs) operate through reversible redox reactions that modulate optical transmittance in response to an electrical potential, enabling real-time control of solar heat and glare while ensuring visual comfort [4–8]. This comfort can even be enhanced using glass-based systems due to their clarity and uniform tinting, but stands out more among ECDs due to the minimal risk of EC layer delamination [9–15]. In the case of large glass-based ECDs, gel polymer electrolytes (GPEs) present notable advantages, namely long-term stability, high transparency, and low risk for leakage [3, 16].

The performance of these ECDs, glass/transparent conductive layer/EC cathode layer/electrolyte/EC anode layer/transparent conductive layer/glass, critically depends on the correspondence between EC materials, electrolyte systems, and interfacial properties [1]. Generally, while ECDs with organic EC materials offer greater color versatility, faster switching, and low long-term stability, inorganic EC materials provide superior durability and stability with limited color options and flexibility [17–19]. For example, a typical inorganic ECD contains metal oxides, such as WO_3 , NiO_x and switches between dark gray and light yellow [5, 16, 20, 21]. Another inorganic EC material is Prussian blue (PB), which is a metal complex and often paired with the hybrid EC material metal coordination polymers (e.g., metal coordination polymer (Fe(II) metal coordination polymer (Fe(II)-MCP))—this ECD changes between a dark blue and a light blue [4, 9, 10, 17, 22–24].

This is an open access article under the terms of the [Creative Commons Attribution](https://creativecommons.org/licenses/by/4.0/) License, which permits use, distribution and reproduction in any medium, provided the original work is properly cited.

© 2026 The Author(s). *ChemElectroChem* published by Wiley-VCH GmbH.

Hence, enhancing cycling stability of ECDs by electrolyte composition can only be demonstrated in conjunction with the EC materials [11, 12, 14, 15, 25, 26]. Moreover, an electrolyte affects response time and cycling stability of ECDs, as the electrolyte has a central role in ECDs, acting as both an ion transport and an electrical insulator layer [2, 26–28]. In addition, the mechanical stability of the electrolyte layer is premise to an operational device [26, 27, 29, 30]. As a result, the required compromise between the high ionic conductivity of a liquid electrolyte and the mechanical stability of a solid electrolyte is a GPE [29, 31]. GPEs, furthermore, combine flexibility with mechanical strength, facilitating an efficient ion exchange within the electrolyte and at the electrode–electrolyte interfaces [1, 32]. Their high ionic conductivity (10^{-3} S·cm $^{-1}$ at 25°C) combined with mechanical stability of a polymer matrix and high transparency (visible light transmittance >90% [26]) are responsible for a fast charge transport and so a uniform color change [25, 29]. Crosslinkers provide another path for optimizing GPE composition by shaping the three-dimensional structure of the polymer network, which in turn directly impacts ionic conductivity, mechanical stability, and electrochemical interface features [33, 34].

The choice of crosslinker determines the change to the GPE composition [33]. Previous research has often focused on using crosslinkers based on polyethylene oxides or epoxy-acrylate in GPEs for ECDs [28, 29, 33]. Despite the recognized importance of crosslinkers in ECD performance, systematic investigations comparing the impact on inorganic versus hybrid ECDs are scarce [12, 27, 35]. The favorable combination of ionic permeability, thermal stability, and compatibility with both inorganic and hybrid EC materials makes poly(propylene glycol) diacrylate (PPGDA) a promising crosslinker [36, 37]. The flexible propylene glycol backbone provides enhanced ionic mobility, while the terminal acrylate groups enable controlled crosslinking density through photopolymerization [38, 39]. PPGDA forms networks (at an average molecular weight of 750 g·mol $^{-1}$) that offer a trade-off between flexibility and crosslinking density [36, 37].

In this context, the clear allocation of what GPE component affects which property of hybrid or inorganic ECD, is paramount: The liquid electrolyte incorporated by the GPE affects the compatibility with the EC electrodes and the ionic transport in the electrolyte layer of the ECD. This can result in a decreased development of charge and transmittance and elongated response times [40]. The choice of polymer matrix of the GPE, here a commercial copolymer of polymethylmethacrylate and polyethylmethacrylate (PB 72), impacts the transparency and the adhesion, which can affect the long-term durability of the ECD [40]. In glass-based ECDs, bubbles can form during assembly and cycling of ECDs [1, 2, 41]. These bubbles can cause nonuniform coloration, reduced optical quality, and potential device failure [36, 42]. Different types of crosslinking systems can modify the structure of the GPE and thus, influence the optical behavior of the ECD and the long-term stabilities [28, 43].

Furthermore, the relationship between PPGDA crosslinking density and key performance metrics such as response time and cycling stability requires detailed elucidation to guide GPE composition design [44–46]. This study addresses this by systematically investigating the influence of PPGDA crosslinker on the EC performance of both inorganic devices (WO $_3$ /NiO $_x$) and hybrid systems (Fe(II)-MCP/PB). Through detailed electrochemical and optical characterization, we aim to reveal structure–property

relationships that enhance switching kinetics and long-term stability of ECDs. The comparative analysis between inorganic and hybrid architectures will provide fundamental insights into crosslinker-material interactions and their implications for next-generation smart glass applications.

Ultimately, the findings suggest PPGDA as crosslinker for ECDs whether of hybrid or inorganic electrode configuration, therefore promoting the growth of energy-efficient smart glass or film technologies in commercial and residential buildings. By optimizing crosslinker for GPEs in glass-based ECDs, this research aspires to meet the demanding performance requirements for smart glass, while ensuring energy-efficient and high-quality devices for large-scale implementation.

2 | Experimental Section

2.1 | Materials and Substrates

The GPE was prepared using LiClO $_4$ (battery grade, dry 99.99% trace metals basis, Merck, Darmstadt, Germany), PC (anhydrous $\geq 99\%$, Merck), DEC (anhydrous $\geq 99.7\%$, Merck), PPGDA average molecular weight of polymer ($M_n = 800$ g·mol $^{-1}$, Sigma-Aldrich, St. Louis, MO, USA), 2,2'-dimethoxy-1,2-diphenylethan-1-one (Irgacure 651 (IRG651), BASF, Ludwigshafen, Germany), and PB 72 (Kremer Pigmente, Aichstetten, Germany). The substrate for the EC electrodes was produced from FTO glass (TEC 15, sheet resistance: ≈ 15 Ω ·sq $^{-1}$) from Pilkington (Lathom, UK). All electrolyte components were stored in an inert environment and used without further purification.

2.2 | Preparation of the Electrolytes

The liquid electrolyte was prepared by dissolving LiClO $_4$ in 50:50 wt% PC:DEC to produce a 1 M transparent colorless solution. The GPE reference was prepared by adding 32.8 wt% PB 72 to the liquid electrolyte and stirring at 25°C for 2 days until a colorless transparent gel was obtained. The polymer:liquid mass ratio was 2:1. The GPE with PPGDA was prepared by adding 5 wt% (relative to the mass of the GPE reference) of PPGDA as a crosslinker; this mixture was stirred for 1 day before adding 4 wt% (relative to the real mass of the crosslinker) of the photoinitiator IRG651 yielding a transparent homogeneous gel. Hereafter, “liquid” and “GPE reference” refer to the liquid electrolyte containing LiClO $_4$ in 50:50 wt% PC:DEC, while the latter refers to the same material but within the PB 72 polymer matrix. “GPE with PPGDA” refers to the electrolyte formulation of the GPE reference plus the PPGDA crosslinker and IRG651 initiator.

2.3 | Characterization of the Electrolytes

2.3.1 | Transmittance

The electrolyte layer was prepared between two microscope slides. The area to be coated with electrolyte was limited using a 50 μ m tape. When preparing the GPE with PPGDA, the sample was cured using a UV lamp (365 nm, Dr. Höhnle AG, UV Technologie, Starnberg, Germany) at a distance of 4 cm for 90 s. The transmittance spectra and color coordinates were recorded using an AvaSpec-2048 standard fiber-optic spectrometer (Avantes,

Apeldoorn, Netherlands) equipped with a balanced deuterium-halogen light source in an inert atmosphere; they are reported following the standards described by the International Commission on Illumination (Vienna, Austria) Lab color space (L^* = lightness, a^* = green-red, b^* = blue-yellow) at 10° and D65 norm. The visible light transmittance (τ_v) is calculated according to DIN EN 410 (Equation S1) [47].

2.3.2 | Ionic Conductivity

The ionic conductivity of the GPEs at different temperatures was determined via electrochemical impedance spectroscopy (EIS) in the noncured state. A symmetrical cell setup (ECC-Std or ECC-REF EL, EL-CELL, Hamburg, Germany) with a glass fiber separator (circle with a diameter of 18 mm, Whatman GF/C, Sigma-Aldrich) was used. The separator was soaked in the electrolyte for 2 h, and the cell was connected to a potentiostat (VMP-300, BioLogic, Seyssinet-Pariset, France) and placed in a climatic chamber (Weiss Klimatechnik, Reiskirchen, Germany). The cell was subjected to the following temperature protocol (all values in $^\circ\text{C}$): 25, 30, 40, 45, 50, 60, 80, 60, 50, 45, 40, 30, 25, 10, 0, -20 , 0, 10, and 25. At each temperature, an open-circuit potential (OCV) step was performed for 30 min to maintain a constant temperature. EIS was conducted in the frequency range from 7 MHz to 100 mHz with an amplitude of 10 mV. The measurement was repeated after another OCV step for 30 min. The first and second measurements showed consistent results at all temperatures, with no significant differences observed. The ionic conductivities were calculated according to Equation S2. The data shown corresponds to the means and standard deviations of at least two cells. The ionic conductivities were calculated and fitted using the Vogel–Tammann–Fulcher equation, according to Equation S3 [48].

2.3.3 | Viscosity

Rheological measurements were performed using a Physica MCR 501 (Anton Paar, Graz, Austria) in viscoelastic mode at 20°C with increasing and decreasing shear rates between 0.1 and 100 s^{-1} . When analyzing the 1 M liquid electrolyte and the GPEs, the plate and cone counterparts were CP15 and PP25 SN23042, respectively. The GPEs were measured in their noncured states. The viscosity η is defined as the ratio of the shear-stress τ and shear deformation γ [49], and the viscosities presented in this study reflect the mean of the fluctuating shear rate of 50 s^{-1} . The adhesion of the GPE reference and GPE with PPGDA is compared by the magnitude of the normal force. The zero-force baseline was calibrated at a gap distance of 1.0 mm, ensuring no mechanical contact or measurable interaction between the plates. The sample was compressed to a gap distance of 0.25 mm and the normal force was recorded while the upper plate was lifted at a controlled rate, generating a force–distance profile. This procedure enabled precise determination of the normal force as a function of the decreasing adhesive interaction with increasing gap distance (Figure S1).

2.3.4 | Preparation of the EC Electrodes and ECDs

The ligand 1,4-bis(2,2':6', 2''-terpyridine-4'-yl)benzene (tpy-ph-tpy = L1) and the metallopolymer Fe(II)-MCP were synthesized according to previously reported procedures. [50, 51]. The Fe(II)-MCP electrodes were prepared via dip coating with a withdrawal speed of $65\text{ mm}\cdot\text{min}^{-1}$ (charge density: $\approx 4.5\text{ mC}\cdot\text{cm}^{-2}$) and

annealed at 60°C for 24 h. PB thin films with nominal charge densities of around $8.0\text{ mC}\cdot\text{cm}^{-2}$ were electrochemically deposited on FTO glass as described by Schott et al. [22]. The deposition of the WO_3 and NiO_x thin film electrodes was conducted as described by Cheng et al. [52], and the electrodes were prepared and provided by Miru Smart Technologies (Vancouver, Canada). Both types of ECDs were contacted on one side with Cu tape.

The Fe(II)-MCP/PB ECDs (size: $5.0\text{ cm} \times 5.0\text{ cm}$, active area: $3.5\text{ cm} \times 4.0\text{ cm}$) were assembled by coating the GPEs onto the Fe(II)-MCP electrodes. A $50\text{ }\mu\text{m}$ spacer tape was used to define the thickness and active area of the electrolyte. The PB electrode was placed on top of the electrolyte after 10 min and the ECD was cured for 90 s at a distance of 4 cm to the UV lamp (365 nm, Dr. Hönle AG, UV Technologie, Starnberg, Germany). The WO_3/NiO_x ECDs (size: $7.5\text{ cm} \times 7.5\text{ cm}$, active area: $6.5\text{ cm} \times 5.0\text{ cm}$) were assembled using the same procedure, except that the GPE was coated on the NiO_x electrode, and the WO_3 electrode was placed on top.

2.3.5 | Characterization of the ECDs

Electrochemical and in-operando spectroelectrochemical measurements of the ECDs were carried out using an Avantes AvaSpec-2048 standard fiber-optic spectrometer with the balanced deuterium-halogen light source and a Multistat 1470E multichannel potentiostat/galvanostat (Solartron Analytical, Farnborough, UK). The UV–vis spectra were recorded during the potentiostatic switching of the ECDs at room temperature, with the voltage applied for 60 s. The operating voltages for bleaching and coloring were chosen to optimize optical performance. The voltages required to switch between the bleached and colored states of the Fe(II)-MCP/PB cells were 0.0 and 2.0 V, respectively, while the voltages required to switch between the colored and bleached states of the WO_3/NiO_x cells were obtained at -1.7 and 1.0 V, respectively. The cycling stability, charge density, and response time were measured by these spectroelectrochemical experiments. The visible light transmittance (τ_v) was calculated according to Equation S1, the charge density was calculated by dividing the measured charge by the active area, and the t_{90} refers to the time required to reach 90% of the maximum change in transmittance at each cycle.

3 | Results and Discussion

3.1 | Electrolyte Characterization

The transparency, ionic conductivity, and mechanical stability are key properties of electrolytes for investigating the effect of GPE composition on ECD performance. The clear allocation of how each component of the GPE takes effect is presented by the comparison of liquid electrolyte, GPE reference, and GPE. In particular, the effect of the polymer PB 72 in the GPE reference in comparison to the liquid electrolyte and the PPGDA crosslinker in comparison to the reference GPE shows the optimization of the GPE formulation.

The high transparency values (τ_v) of the liquid electrolyte (92%), GPE reference (92%), and GPE with PPGDA (93%), ensure high clarity in ECD, which is essential for their effective use in smart windows (Figure 1A) [26]. The transparency depends on their composition and thickness [53]. Adding the polymer matrix

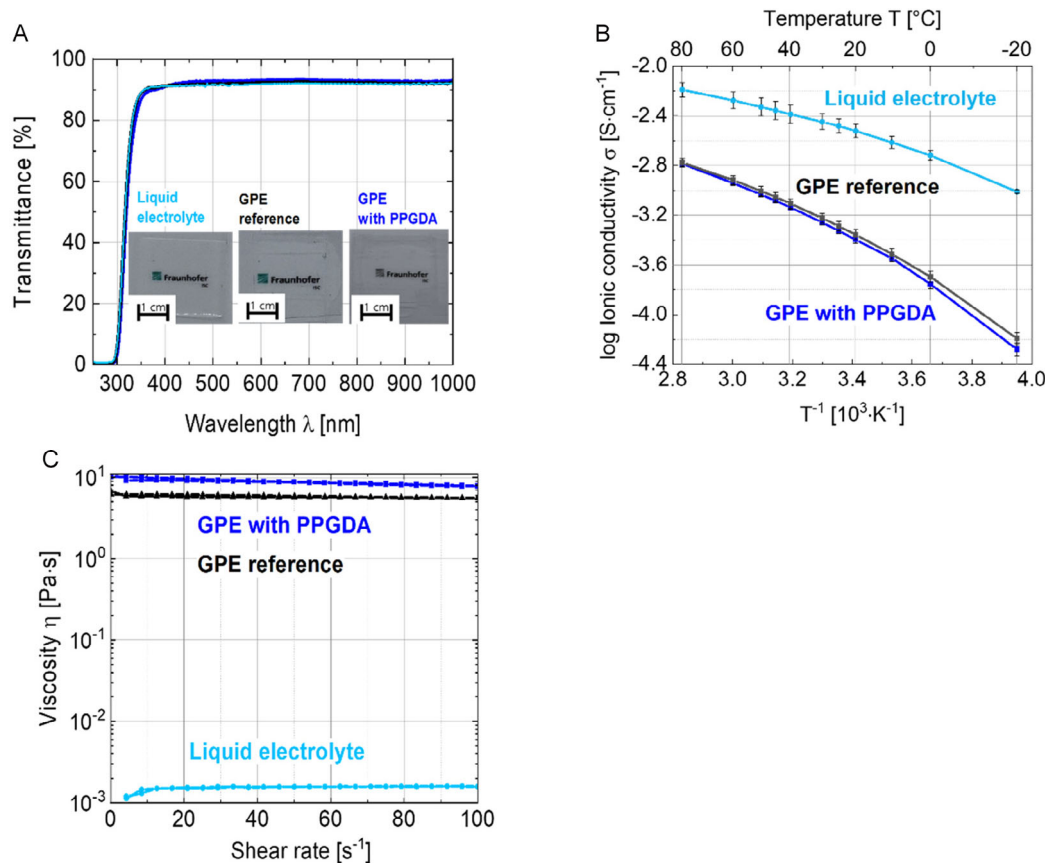


FIGURE 1 | Characterization of the liquid electrolyte, GPE reference, and GPE with PPGDA. (A) Transmittance spectra and photographs between two microscope slides (thicknesses of the electrolyte layer: 50 μ m). (B) Temperature-dependent ionic conductivities. (C) Viscosity measurements.

PB 72 to the liquid electrolyte for the GPE reference and the PPGDA for the GPE maintains transparency at a layer thickness of 50 μ m. As a result, GPE reference and GPE with PPGDA show suitable transparencies for ECDs.

The temperature-dependent ionic conductivity of the electrolytes was measured from -20 to $80^{\circ}C$ (Figure 1B). At the ECD cycling temperature of $25^{\circ}C$, the liquid electrolyte exhibits an ionic conductivity of $3.3 \times 10^{-3} S \cdot cm^{-1}$, the GPE reference $5.1 \times 10^{-4} S \cdot cm^{-1}$, and the GPE with PPGDA $4.8 \times 10^{-4} S \cdot cm^{-1}$. The lower ionic conductivities of the GPEs compared to the liquid electrolyte can be attributed to reduced charge mobilities due to the addition of the polymer matrix PB 72. Notably, the ionic conductivity of the GPE reference was similar to that of the GPE with PPGDA, suggesting that the PPGDA crosslinker does not significantly affect the ionic conductivity. The ionic conductivity of the liquid electrolyte is primarily determined by salt concentration, which generally peaks at 1 M [54]. $LiClO_4$ is chosen for its high Li mobility and its compatibility with the Fe(II)-MCP electrode, as the perchlorate anion is inserted into it. The binary solvent (50:50 wt% PC:DEC) balances the low viscosity of the linear ester (DEC) with the high dielectric constant of the cyclic ester (PC) [55].

The mechanical stability of the electrolytes is assessed by their viscosities. Viscosities of the electrolytes were measured in their noncured states (Figure 1C). Increasing solid polymer content results in higher viscosities; the viscosities of the samples in ascending order were as follows liquid electrolyte (1.5 mPa·s) < GPE reference (5.8 Pa·s) < GPE with PPGDA (8.7 Pa·s). The GPE with PPGDA exhibited the highest viscosity due to the distribution of

the acrylic monomer throughout the electrolyte [56, 57]. The magnitude of the normal force of the GPE reference at -33.2 N is lower than the one of the GPE with PPGDA at -36.2 N. The tackiness is therefore higher for the GPE with PPGDA and leads to a better adhesion between the EC electrodes of the cell (Figure 1).

While the addition of the polymer matrix enhances the mechanical stability of the electrolyte layer, it also increases viscosity, which can lower the charge mobility. This mechanical stability is crucial for maintaining long-term contact between the electrodes and facilitating ion transport. The shear viscosity analysis indicates that viscosity can be adjusted for processability through the polymer matrix PB 72 and crosslinker PPGDA [58]. Furthermore, the exposure to light initiates the in situ polymerization of the crosslinking system, resulting in increased viscosity and adhesion [59].

As the liquid electrolyte demonstrates high transparency and ionic conductivity, the analysis reveals that both GPEs (reference and with PPGDA) exhibit higher mechanical stability, which is important for the application in ECDs. The higher mechanical stability may decrease ionic conductivity. Thus, it is necessary to compare GPE reference and GPE with PPGDAs in ECDs to understand their effect on the overall device performance.

3.2 | Investigation of the Crosslinker PPGDA Impact on Fe(II)-MCP/PB and WO_3/NiO_x ECDs

The GPE reference and GPE with PPGDA were evaluated in two different ECD configurations: a hybrid (Fe(II)-MCP/PB) and an

inorganic ECD (WO_3/NiO_x). The impact of the PPGDA cross-linker on the key parameters such as transmittance, t_{90} , and cycling stability is examined to determine how PPGDA impacts this electrolyte formulation [6, 26, 60].

3.3 | Hybrid ECD System: Fe(II)-MCP/PB

The detailed electrochemical characterization and preparation of the Fe(II)-MCP and PB electrodes were previously described by Schott et al. [22]. The anode (PB on FTO glass) exhibits a higher charge density ($8.0 \text{ mC}\cdot\text{cm}^{-2}$) than that of the cathode Fe(II)-MCP on FTO glass $4.5 \text{ mC}\cdot\text{cm}^{-2}$. The over-dimensioned PB layer provides enough charge and improves the cycling stability without affecting the t_{90} . Furthermore, their overall charge is limited by the electrode with the lower charge density [23]. The Fe(II)-MCP/PB ECDs were cycled between their bleached (2.0 V) and colored (0.0 V) states for 60 s at room temperature. The performance of the ECD was evaluated in terms of transmittance, cycling stability, and t_{90} [48, 61, 62]. The contrast ratio (CR) and coloration efficiency (CE) were determined using Equations S4 and S5.

The comparison of the transmittance spectra of the Fe(II)-MCP/PB ECDs with the GPE reference and the GPE with PPGDA (Figure 2A,B) shows a general increase of the τ_v values during cycling for bleached (GPE reference: 44% to 61%, GPE with PPGDA: 43% to 61%) and colored (GPE reference: 8% to 11%, GPE with PPGDA: 10% to 16%) state. The photographs of the ECDs shown in Figure 2C,D depict the full-area color changes and highly transparent and uniform GPEs. Furthermore, no

bubble formation was observed in the GPEs before or after cycling. The $L^*a^*b^*$ color coordinates are summarized in Table S1. The $L^*a^*b^*$ values of the ECD with the reference GPE in the bleached and colored state increase from 72.5 to 82.3 and from 36.4 to 41.7, respectively. The ECD with the PPGDA-modified electrolyte shows a similar behavior with $L^*a^*b^*$ increasing from 72.1 to 82.5 in the bleached state and the colored state changing from 39.5 to 49.1.

Both ECDs exhibit an overall stable charge density (Figure 3A) over 1000 switching cycles, with the ECD with GPE reference having slightly higher values (4.8 to $4.9 \text{ mC}\cdot\text{cm}^{-2}$) compared to GPE with PPGDA (3.9 to $4.2 \text{ mC}\cdot\text{cm}^{-2}$). Notably, the higher charge densities of the ECDs slightly increase during cycling. In contrast, the optical characterization is showing a significant increase in τ_v (Figure 3B) during cycling. The initial transmittance modulation between the colored and bleached state of the ECDs with both electrolyte formulations is quite similar and increases during cycling: From $\Delta\tau_v = 22\%$ (16/38%) in the 5th cycle to 33% (22-55%) in the 1000th cycle for the GPE reference and from $\Delta\tau_v = 19\%$ (20/39%) to 32% (24/56%) for the GPE with PPGDA. Thus, the Fe(II)-MCP/PB ECDs with both GPEs ensure a good cyclability over 1000 cycles.

The Fe(II)-MCP/PB ECD with the GPE reference exhibits t_{90} values of 10/7 s for bleaching/coloring in the 5th cycle, which increase to 43/13 s after 1000 cycles (Table 1). In comparison, the ECD containing the GPE with PPGDA demonstrates initial t_{90} values of 9/8 s in the 5th cycle and a significant drop in the bleaching t_{90} to 43 s by the 1000th cycle, while the coloring response elongates to 16 s. Although both GPEs show

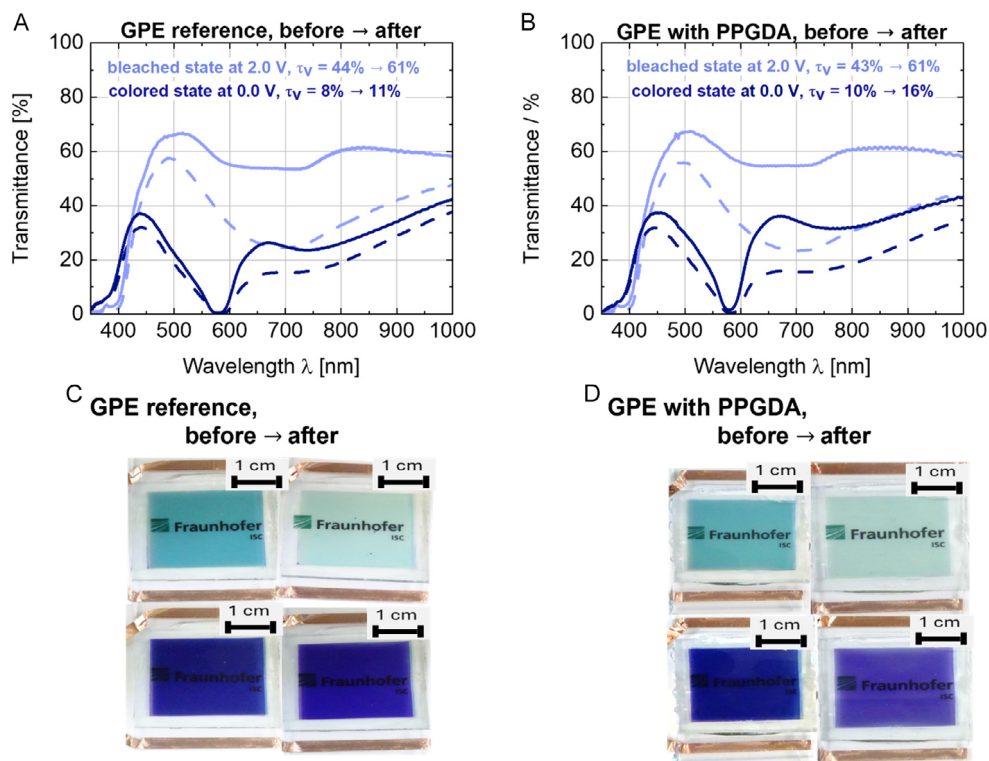


FIGURE 2 | Transmittance spectra before (dashed lines) and after (solid lines) 1000 cycles for (A) GPE reference and (B) GPE with PPGDA in Fe(II)-MCP/PB ECDs (active area: $4.5 \text{ cm} \times 3.0 \text{ cm}$). Photographs of the ECDs with (C) GPE reference and (D) GPE with PPGDA before (left column) and after 1000 cycles (right column).

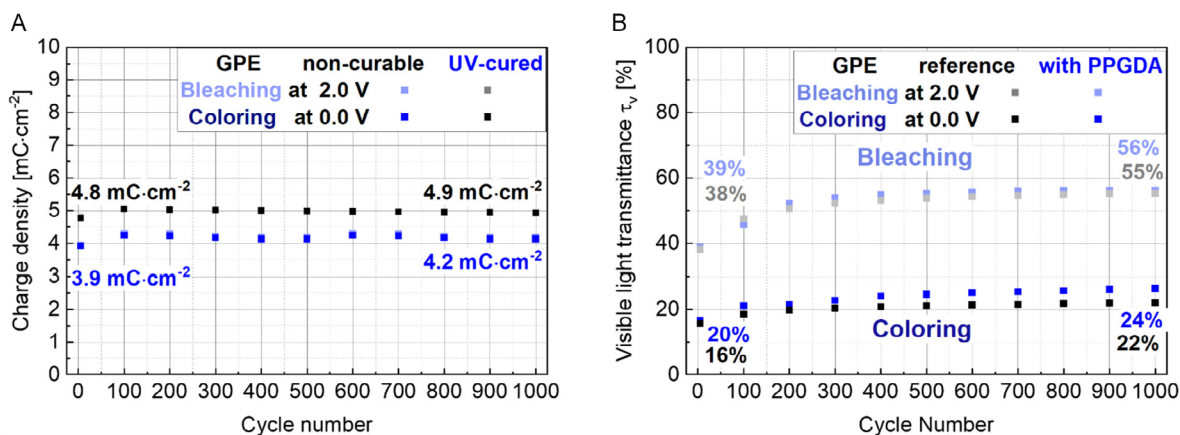


FIGURE 3 | Fe(II)-MCP/PB ECDs with GPE reference (black) and GPE with PPGDA (blue) in the colored and bleached states at 0.0 and 2.0 V, respectively (voltage applied for 60 s). (A) Charge densities over 1000 switching cycles including charge/discharge densities in the 5th and 1000th cycle. (B) τ_v values (colored/bleached) over 1000 cycles including transmittance values of the colored and bleached states in the 5th and 1000th cycle.

TABLE 1 | Characteristic EC properties of the Fe(II)-MCP/PB ECDs (4.0 cm × 3.5 cm) at cell voltages of 0.0/2.0 V (colored/bleached) and the WO₃/NiO_x ECDs (6.5 cm × 5.0 cm) at cell voltages of -1.7/1.0 V (colored/bleached). The λ_{\max} values of the Fe(II)-MCP/PB and WO₃/NiO_x ECDs are 586 and 800 nm, respectively.

	Fe(II)-MCP/PB ^a 4.0 cm × 3.5 cm				WO ₃ /NiO _x 6.5 cm × 5.0 cm			
	reference		with PPGDA		reference		with PPGDA	
Electrolyte (GPE)	reference		with PPGDA		reference		with PPGDA	
Cell voltage (V)	0.0	2.0	0.0	2.0	-1.7	1.0	-1.7	1.0
	colored bleached		colored bleached		colored bleached		colored bleached	
Transmittance at λ_{\max} (5 th /1000 th cycle) (%)	0.2/1	38/51	1/2	47/60	26/23	92/59	37/48	100/84
Contrast ratio (5 th /1000 th cycle) ^a	162.4/63.6		42.2/59.4		3.7/2.9		2.7/1.8	
Charge density (5 th /1000 th cycle) (mC·cm ⁻²)	4.8/4.9		3.9/4.2		8.9/4.9		6.6/3.0	
Coloration efficiency (5 th /1000 th cycle) (cm ² ·C ⁻¹)	459/365		382/452		63/95		66/82	
Response time t_{90} (5 th /1000 th cycle) (s)	7/13	10/43	9/16	8/43	47/39	44/38	54/52	33/24

^aThe contrast ratio was calculated with exact values.

comparable performance in initial cycles, the incorporation of PPGDA results in enhanced bleaching speed due to the cross-linked structure of GPE with PPGDA, which probably facilitates faster ion migration during EC switching. This leads to quicker coloration and bleaching. However, both GPEs exhibit increased t_{90} values after 1000 cycles, indicating that while PPGDA enhances performance, the long-term cycling effects impact t_{90} for both formulations (Figure S2A,B, and S3A,B). Overall, the presence of PPGDA contributes positively to the t_{90} , underscoring its significance in optimizing GPE compositions for ECDs.

Combining the findings of charge density and τ_v presents the GPE with PPGDA needing less charge density while exhibiting higher transparency values in contrast to the GPE reference. The more detailed analysis of current and charge density for bleached and colored state adds to that, as the GPE with PPGDA is showing a lower charge density (Figures S4 and S5). Although, the GPE with PPGDA has the higher mechanical stability, the charge transport seems to be stabilized by the crosslinked network. A possible explanation would be that PPGDA establishes an environment with improved local concentration, migration,

and convection gradients [63]. These confined spaces within the macromolecular network can facilitate accelerated charge transport through the GPE [64].

The redox processes responsible for the color changes in the ECD occur at the electrodes. While in their bleached state of the Fe(II)-MCP/PB ECDs, the perchlorate anions are inserted into the cathodic Fe(II)-MCP layer and the Li⁺ cations are inserted into the PB electrode [65]. The insertion of these ions results in a smaller highest occupied molecular orbital-lowest unoccupied molecular orbital (HOMO–LUMO) gap, thus resulting in a brighter appearance. The transmittance spectra of both Fe(II)-MCP/PB ECDs in the bleached and colored states exhibit increased τ_v values after cycling. This increase prominent between 650–900 nm suggests that the number of electron transitions in PB (i.e., the characteristic peak of PB is observed at 700 nm) is increasing. Figures S4 and S5 show the changes in the current and charge densities over 1000 cycles. Notably, after the 5th cycle, the observed charge density plateau during bleaching at 2.0 V, which describes the decreasing efficiency of the cell to change color, for the GPE with PPGDA is less pronounced than for the GPE reference. Unlike coloring,

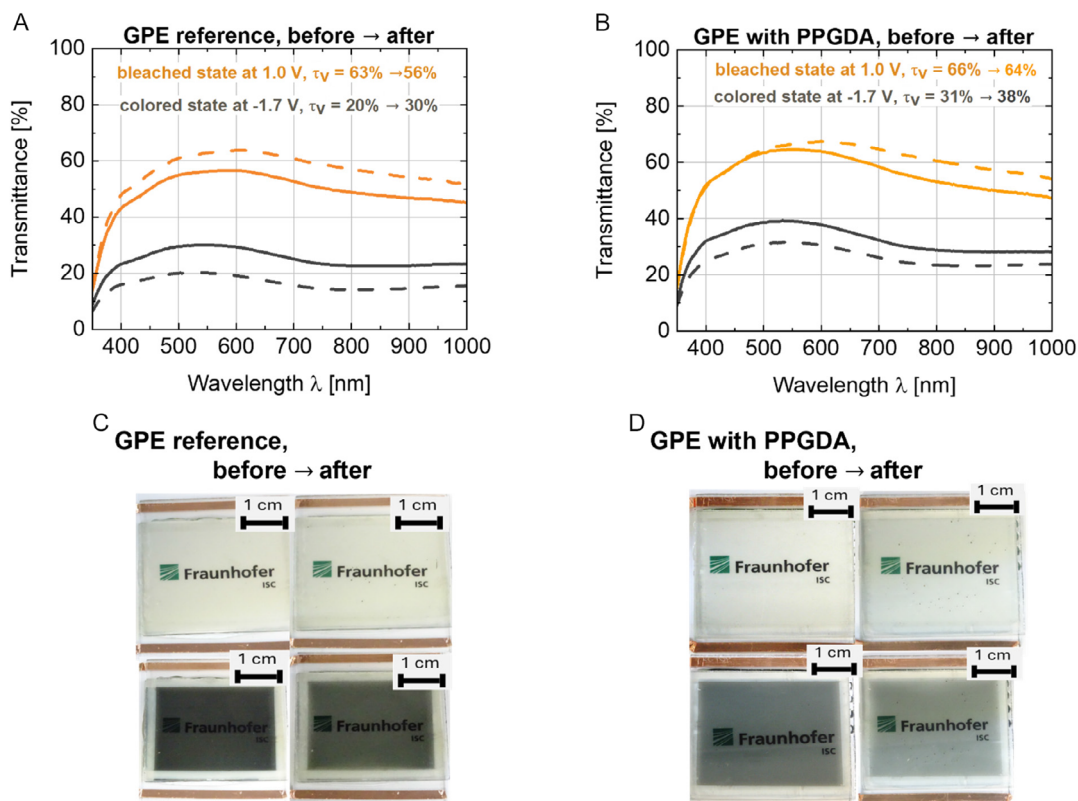


FIGURE 4 | Transmittance spectra before (dashed lines) and after (solid lines) 1000 cycles for (A) GPE reference and (B) GPE with PPGDA in WO_3/NiO_x ECDs (active area: 6.5 cm \times 5.0 cm). Photographs of the ECDs with (C) GPE reference and (D) GPE with PPGDA before (left column) and after 1000 cycles (right column).

bleaching shows a plateau in the charge density, after which the bleaching process occurs abruptly; this threshold varies with continuous cycles.

3.4 | Inorganic ECD System: WO_3/NiO_x

The WO_3/NiO_x ECDs were cycled between their bleached (1.0 V) and colored (-1.7 V) states, with the potentials applied for 60 s at room temperature under inert conditions. The detailed electrochemical characterization of the WO_3 and NiO_x electrodes has been previously described by Cheng et al. [52].

Both ECDs demonstrate a reasonable cycling stability over 1000 switching cycles. However, an overall decrease of the τ_v values in both ECDs is observed, when comparing the transmittance spectra before and after cycling (Figure 4A,B). Although the initial transmittance values, in particular in the colored state, are different for both ECDs (GPE reference: 20/63%, GPE with PPGDA: 31/66%), the overall transmittance change ($\Delta\tau_v = 26\%$) after cycling is identical (Figure 4B). This indicates that the GPE with PPGDA does not change the optical behavior of the ECDs. The $L^*a^*b^*$ color coordinates of the WO_3/NiO_x ECDs are summarized in Table S1. The photographs of the ECDs show that no bubbles are visible before and after 1000 cycles, highlighting the stability of the GPE with PPGDA (Figure 4C,D).

The charge density of the ECDs containing GPE with PPGDA decreases from 6.6 to 3.0 $\text{mC}\cdot\text{cm}^{-2}$, while the charge density of the GPE reference drops from 8.9 to 4.9 $\text{mC}\cdot\text{cm}^{-2}$ (Figure 5A). The ECDs with the GPE with PPGDA has lower charge density

than the ECD with the GPE reference over 1000 cycles. However, the trend is similar for both GPEs and corresponds with the change of the transmittance values.

The comparison of the optical properties during cycling demonstrates a smaller decrease in the bleached state transmittance from 65% (5th cycle) to 58% (1000th cycle) for the GPE with PPGDA, which indicates only a 7% darkening, while the GPE reference has a 10% darkening with values of 62% and 52% (Figure 5B), respectively. The behavior after 1000 cycles for the colored state is quite similar, although it increases for the GPE with PPGDA from 27% to 35% and from 20% to 28% for the GPE reference.

The time-dependent charge and current densities of the WO_3/NiO_x ECDs during bleaching and coloring (Figures S8 and S9) reveal that the charge densities in subsequent cycles increase more significantly with the GPE reference compared to those observed with the GPE containing PPGDA. The charge density and τ_v behavior over 1000 cycles found in Figure 5 collectively support that the additional PPGDA alters the charge transport for the WO_3/NiO_x ECDs.

The WO_3/NiO_x ECDs with the GPE reference exhibit t_{90} values of 44 s for bleaching and 47 s for coloring in the 5th cycle, which decrease to 38 s for bleaching and 39 s for coloring at the 1000th cycle (Table 1). In contrast, the ECDs with the GPE containing PPGDA displayed improved initial t_{90} values of 33 s for bleaching and 54 s for coloring, decreasing to 24 s for bleaching and 52 s for coloring after 1000 cycles. This data indicates that while both GPEs show a decrease in bleaching times after

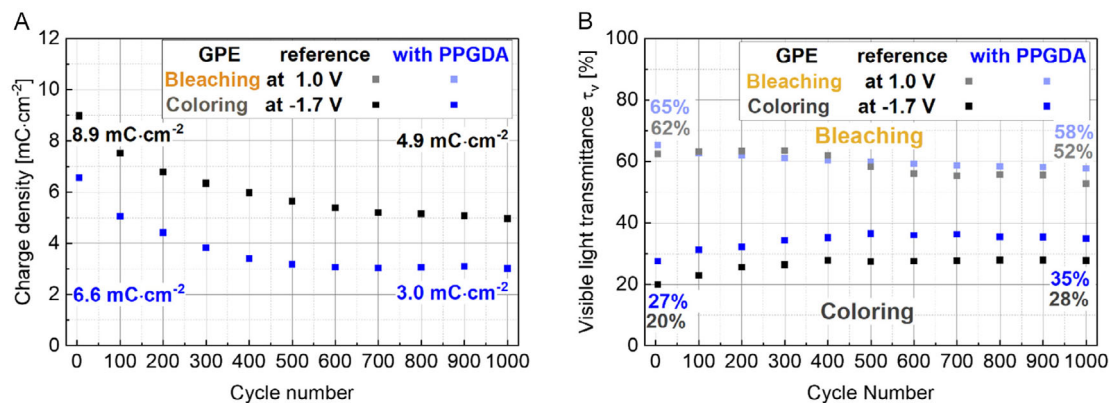


FIGURE 5 | GPE reference (black) and GPE with PPGDA (blue) in the WO₃/NiO_x ECDs with their respective coloration and discoloration potentials at -1.7 and 1.0 V applied for 60 s. (A) Charge densities over 1000 switching cycles including charge/discharge densities in the 5th and 1000th cycle. (B) τ_v values (colored/bleached) over 1000 cycles including transmittance values of the colored and bleached states in the 5th and 1000th cycle.

cycling. The GPE with PPGDA consistently enhances EC performance by facilitating faster transitions between the bleached and colored states (Figures S6A,B, and S7A,B). Thus, the incorporation of PPGDA not only improves t_{90} at 5th cycle for bleaching but also contributes to maintaining better performance over cycling compared to the GPE reference.

The τ_v values of the ECDs in the bleached and colored states are strongly associated with their charge densities and exhibit similar trends over 1000 cycles. Charge transfers induce optical changes in the ECDs. Cycling stability of the ECDs is influenced by their electrochemical stability, which is dependent on the charge densities and surface structures of the electrodes [52]. In the bleached state, the WO₃ electrode is reduced from W⁶⁺ to W⁵⁺, whereas the NiO_x electrode is oxidized due to the introduction of Li⁺. In the colored state, Li⁺ is introduced to the WO₃ electrode, reducing W⁶⁺ to W⁵⁺, while the Ni²⁺ within the NiO_x electrode is oxidized to Ni³⁺ and Ni⁴⁺. The bleaching and coloring involve alternating Li⁺ insertion and extraction from the WO₃ and NiO_x layers [21, 52, 66]. Despite the different charge densities of the ECDs, the transmittance gap between bleached and colored is quite similar for the two shown WO₃/NiO_x ECDs.

3.5 | Similarities and Differences of the GPE with PPGDA in the Fe(II)-MCP/PB and WO₃/NiO_x ECDs

While the response times, optical stability, and charge densities of both WO₃/NiO_x and Fe-MCP/PB ECDs benefit from the inclusion of PPGDA in the GPE, the effects on CE and CR by the PPGDA crosslinker are dependent on each kind of ECD. Nevertheless, the differences of CE and CR inside each ECD system highlight the optimization potential of the specific EC materials in conjunction with the GPE (Table 1).

The ratio of bleached over colored transmittance at maximal absorbance is the CR (Equation S4) and aligns to the changes in transmittance during cycling. For the Fe(II)-MCP/PB ECDs, the CR decreases during cycling and lower for the GPE with PPGDA, although it is higher at the 5th cycle. For the WO₃/NiO_x the CR is much lower than for the Fe(II)-MCP/PB ECDs and slightly decreases after cycling (3.7 to 2.9 for the GPE reference and 2.7 to 1.8 for the GPE with PPGDA). As the CR is mainly dependent on the used EC materials, the GPE affects this

parameter by changing the electrochemical state of the layers after cycling.

The CE is the ratio of CR over the inserted/extracted charge (Equation S5) and is a standard method to characterize the optical change induced by the applied potential [48, 67]. Higher CEs indicate improved performance, requiring less energy for significant color changes [20]. For the Fe(II)-MCP/PB ECDs, the difference in CE from 459 to 365 cm²·C⁻¹ with GPE reference is higher than from 382 to 452 cm²·C⁻¹ with PPGDA. In comparison, the WO₃/NiO_x ECD with the GPE reference exhibits a CE increase from 63 to 95 cm²·C⁻¹ and the GPE with PPGDA from 66 to 82 cm²·C⁻¹. The relationship between the type of GPE and CE in the WO₃/NiO_x cell increases after 1000 cycles. Although the CE is an inevitable parameter when discussing the performance of ECDs, the observed difference of CEs between the GPEs seems to be mainly affected by the different charge transport of the GPEs.

It is essential to differ between the effects of the GPE and the effect of the different EC materials, when the impact of the GPE with PPGDA on these two different ECD types is summarized. The two different GPEs have high transparencies (Figure 1A) while exhibiting relatively similar ionic conductivities (Figure 1B). Furthermore, the GPE with PPGDA shows increased mechanical stability in contrast to the GPE reference (Figure 1C). Although the higher mechanical stability should impede the charge transport, the GPE with PPGDA exhibited in both ECD types favorable cycling stability and response times.

Charge densities decrease during cycling, while for both, Fe(II)-MCP/PB and WO₃/NiO_x, the ECDs containing the GPE with PPGDA showed lower charge densities overall in comparison with the GPE reference. For the optical performance, the hybrid EC system increased its transparency, shown by higher τ_v value, and the inorganic EC system decreased over 1000 cycles, but they had in common that the GPE with PPGDA shows higher transparency and more stable τ_v . The t_{90} depicts the difference between Fe(II)-MCP/PB and WO₃/NiO_x in coloration mechanism quite clear, as it elongates for the Fe(II)-MCP/PB over cycling and stays even or shortens for the WO₃/NiO_x ECDs. This is even more significant, when pointing out the active area of WO₃/NiO_x (6.5 cm × 5.0 cm) being larger than the one of Fe(II)-MCP/PB (4.0 × 3.5 cm).

The observed optical and electrochemical stability and the t_{90} demonstrate that the structure, created by the PPGDA in the electrolyte, affects ion transport [36, 39, 42]. In particular, the WO_3/NiO_x incorporating the GPE with PPGDA benefits by shorter response times and lower charge densities at maintaining almost the same optical characteristics as the cell with GPE reference. The comparison of the charge and current densities during cycling (Figures S4 and S5 for Fe(II)-MCP/PB and Figures S8 and S9 for WO_3/NiO_x) show that the (dis-)charging behavior during the presented 1000 cycles of GPE reference and GPE with PPGDA is independent on the EC materials. Obviously, bleaching and coloring is triggered by charging and discharging. So, the resulting t_{90} values of the ECDs reveal that the optimization of the t_{90} depends on the correspondence between GPE and the EC electrodes.

4 | Conclusion

In this study, the impact of the PPGDA crosslinker within a polymer matrix for glass-based ECDs with regard to the cycling stability, charge density, and response time is investigated. The key findings demonstrate that the crosslinker PPGDA within the PB 72 polymer matrix enhances the mechanical stability of the GPE with minimal decreasing of ionic conductivity. The comparative analysis of GPE reference and GPE with PPGDA across both hybrid Fe(II)-MCP/PB and inorganic WO_3/NiO_x ECDs highlights the advantages of the PPGDA crosslinker in influencing charge density, transmittance modulation, and response time of ECDs during cycling.

Notably, the GPE with and without PPGDA exhibited similar optical properties and cycling stability over 1000 cycles alongside lower charge densities. In terms of response times the behavior of the ECDs containing the GPE reference and the GPE with PPGDA correlates with the change in the optical and electrochemical properties. The PPGDA crosslinker has obviously no negative effect on the long-term cycling stability of the ECDs but slightly influences the coloring and bleaching times. These findings imply that the behavior of various EC materials can vary considerably depending on operating conditions and the specific configuration of the ECD.

Future optimization efforts should concentrate on exploring the macromolecular structures generated by crosslinkers within diverse polymer matrices. Although modifying the liquid electrolyte could enhance ionic transport, this approach is not suitable for Fe(II)-MCP/PB ECDs due to their reliance on perchlorate anions for coloration. In contrast, such modifications remain feasible for WO_3/NiO_x ECDs. Additionally, investigating alternative crosslinkers for use in PMMA- or PEMA-based (PB 72) polymers could uncover beneficial charge transport and stabilization properties. Addressing these areas will be interesting for developing commercially viable ECDs that feature shorter response times and enhanced durability.

While these findings underscore the influence of EC materials on performance, it appears that these effects may be less pronounced than initially hypothesized. Nonetheless, further investigation into the role of crosslinkers in GPE composition is essential, as gaining additional insights into the structure of cured GPEs will be crucial for future optimization efforts. This work lays the groundwork for enhancing the performance characteristics

of ECDs by appropriate crosslinker, ultimately contributing to their practical applications in smart window technologies.

Author Contributions

Selma Dahms: conceptualization (equal); investigation (lead); methodology (lead); visualization (lead); writing—original draft (lead). **Lukas Niklaus:** conceptualization (supporting); investigation (supporting); methodology (supporting); project administration (supporting); validation (supporting); writing—original draft (supporting). **Marco Schott:** conceptualization (equal); funding acquisition (lead); methodology (supporting); project administration (lead); supervision (lead); validation (supporting); writing—review & editing (lead).

Acknowledgments

The authors are grateful to the Federal Ministry of Education and Research for funding the German–Canadian collaborative project FLAIM (grant no. 01DM21002C). The authors would like to acknowledge Miru Smart Technologies for providing the WO_3 and NiO_x electrodes.

Open Access funding enabled and organized by Projekt DEAL.

Funding

This study was supported by Bundesministerium für Bildung und Forschung (Grant 01DM21002C).

Conflicts of Interest

The authors declare no conflicts of interest.

References

1. C. Hu, L. Li, J. Zhou, B. Li, S. Zhao, and C. Zou, “Enhanced Contrast of WO_3 -Based Smart Windows by Continuous Li-Ion Insertion and Metal Electroplating,” *ACS Applied Materials & Interfaces* 14 (2022): 32253.
2. G. K. Silori, S. Thoka, and K.-C. Ho, “Demonstration of a Gel-Polymer Electrolyte-Based Electrochromic Device Outperforming Its Solution-Type Counterpart in All Merits: Architectural Benefits of CeO_2 Quantum Dot and Nanorods,” *ACS Applied Materials & Interfaces* 16 (2024): 4958.
3. S. Lashgari and M. H. Jahangir, “A Comparative Analysis of Thermal Comfort, Energy Consumption, Pollutant Emissions, and Visual Comfort in a School Building Utilizing Electrochromic and Thermo-chromic Windows,” *Energy Strategy Reviews* 60 (2025): 101772.
4. Y. Alesanco, J. Palenzuela, R. Tena-Zaera, et al., “All-in-One Gel-Based Electrochromic Devices: Strengths and Recent Developments,” *Solar Energy Materials and Solar Cells* 157 (2016): 624.
5. K. Ahmad, G. Song, and H. Kim, “Fabrication of Tungsten Oxide/Graphene Quantum Dot (WO_3 @GQD) Thin Films on Indium Tin Oxide-Based Glass and Flexible Substrates for the Construction of Electrochromic Devices for Smart Window Applications,” *ACS Sustainable Chemistry & Engineering* 10 (2022): 11948.
6. C. Y. Jeong, T. Kubota, K. Tajima, M. Kitamura, and H. Imai, “Complementary Electrochromic Devices based Acrylic Substrates for Smart Window Applications in Aircrafts,” *Materials Chemistry and Physics* 277 (2022): 125460.
7. C. Lee, Y. Oh, I. S. Yoon, S. H. Kim, B.-K. Ju, and J.-M. Hong, “Flash-Induced Nanowelding of Silver Nanowire Networks for Transparent Stretchable Electrochromic Devices,” *Scientific Reports* 8 (2018): 2763.
8. S.-J. Oh and J. W. Bae, “All-in-One Plasticized Lonogel-based Stretchable Electrochromic Devices,” *Chemical Engineering Journal* 467 (2023): 143367.

9. S. Macher, M. Schott, M. Dontigny, "Large-Area Electrochromic Devices on Flexible Polymer Substrates with High Optical Contrast and Enhanced Cycling Stability," et al., *Advanced Materials Technologies* 6 (2021): 2000836.
10. V. Bayzi Isfahani and M. M. Silva, "Fundamentals and Advances of Electrochromic Systems: A Review," *Advanced Engineering Materials* 23 (2021): 2100567.
11. P. Yang, P. Sun, and W. Mai, "Electrochromic Energy Storage Devices," *Materials Today* 19 (2016): 394.
12. Z. Wang, H. Zhu, J. Zhuang, Y. Lu, Z. Chen, and W. Guo, "Recent Advance in Electrochromic Materials and Devices for Display Applications," *ChemPlusChem* 89 (2024): e202300770.
13. S. Macher, M. Rumpel, M. Schott, U. Posset, G. A. Giffin, and P. Löbmann, "Avoiding Voltage-Induced Degradation in PET-ITO-Based Flexible Electrochromic Devices," *ACS Applied Materials & Interfaces* 12 (2020): 36695.
14. E. S. Lee and A. Tavil, "Energy and Visual Comfort Performance of Electrochromic Windows with Overhangs," *Building and Environment* 42 (2007): 2439.
15. A. Cannavale, U. Ayr, F. Fiorito, and F. Martellotta, "Smart Electrochromic Windows to Enhance Building Energy Efficiency and Visual Comfort," *Energies* 13 (2020): 1449.
16. A. Kraft, "Is there a Crisis in the Smart Glass Industry?," *Solar Energy Materials and Solar Cells* 284 (2025): 113487.
17. M. Higuchi, "Electrochromic Organic–Metallic Hybrid Polymers: Fundamentals and Device Applications," *Polymer Journal* 41 (2009): 511.
18. Z. Wang, X. Wang, S. Cong, et al., "Towards Full-colour Tunability of Inorganic Electrochromic Devices using Ultracompact Fabry-perot Nanocavities," *Nature Communications* 11 (2020): 302.
19. L. Huang, S. Cao, Y. Liang, et al., "Advances in Multicolor Electrochromic Devices based on Inorganic Materials," *Journal of Materials Chemistry C* 11 (2023): 10107.
20. S. Heo, C. J. Dahman, C. M. Staller, et al., "Enhanced Coloration Efficiency of Electrochromic Tungsten Oxide Nanorods by Site Selective Occupation of Sodium Ions," *Nano Letters* 20 (2020): 2072.
21. G. Atak, S. Ghorai, C. G. Granqvist, G. A. Niklasson, and I Bayrak Pehlivan, "Cycling Durability and Potentiostatic Rejuvenation of Electrochromic Tungsten Oxide Thin Films: Effect of Silica Nanoparticles in LiClO₄-Propylene Carbonate Electrolytes," *Solar Energy Materials and Solar Cells* 250 (2023): 112070.
22. M. Schott, L. Niklaus, C. Müller, B. Bozkaya, and G. A. Giffin, "Flexible Electrochromic Devices Prepared on Ultra-thin ITO Glass," *Materials Advances* 2 (2021): 4659.
23. L.-C. Chen and K.-C. Ho, "Design Equations for Complementary Electrochromic Devices: Application to the Tungsten Oxide–Prussian Blue System," *Electrochimica Acta* 46 (2001): 215.
24. M. Schott, L. Niklaus, S. Janietz, C. Völkel, T. Egorov-Brening, and T. Bilkay-Troni, "Electropolymerization of an EDOT-Quinoxaline Monomer for Green Electrochromic Thin Films and Devices," *Polymers* 16 (2024): 799.
25. X. Cheng, J. Pan, Y. Zhao, M. Liao, and H. Peng, "Gel Polymer Electrolytes for Electrochemical Energy Storage," *Advanced Energy Materials* 8 (2018): 1702184.
26. V. Primiceri, M. Pugliese, C. T. Prontera, et al., "Low-cost Gel Polymeric Electrolytes for Electrochromic Applications," *Solar Energy Materials and Solar Cells* 240 (2022): 111657.
27. W. Chen, C. Zhu, M. Yan Le Guo, et al., "A Novel Ionically Crosslinked Gel Polymer Electrolyte as an ion Transport Layer for High-performance Electrochromic Devices," *Journal of Materials Chemistry C* 7 (2019): 3744.
28. B. Boz, T. Dev, A. Salvadori, and J. L. Schaefer, "Review—Electrolyte and Electrode Designs for Enhanced Ion Transport Properties to Enable High Performance Lithium Batteries," *Journal of The Electrochemical Society* 168 (2021): 090501.
29. X. Zhang, J. Tian, and C. Jia, "Advances in the Study of Gel Polymer Electrolytes in Electrochromic Devices," *Journal of Progress in Engineering and Physical Science* 2 (2023): 47.
30. Z. Zhou, Y. Tang, F. Zhao, et al., "Transparent Succinonitrile-modified Polyacrylate Gel Polymer Electrolyte for Solid Electrochromic Devices," *Chemical Engineering Journal* 481 (2024): 148724.
31. B. O. Orimolade and E. R. Draper, "Application of Quasi Solid Electrolytes in Organic based Electrochromic Devices: A Mini Review," *Chemistry-A European Journal* 30 (2024): e202303880.
32. Q. Wang, P. Zhang, W. Zhu, et al., "A Two-step Strategy for Constructing Stable Gel Polymer Electrolyte Interfaces for Long-life Cycle Lithium Metal Batteries," *Journal of Materiomics* 8 (2022): 1048.
33. H. Afshar, F. Kamran, and F. Shahi, "Advances in Smart Chromogenic Hydrogel Composites for Next-Generation Digital Applications," *Polymers for Advanced Technologies* 36 (2025): e70179.
34. Y. Wang, X. Sun, Q. Liu, and G. Yu, "Functional Gel Materials for Next-generation Electrochromic Devices and Applications," *Chemical Society Reviews* 54 (2025): 3475.
35. W. Wang, S. Guan, M. Li, J. Zheng, and C. Xu, "A Novel Hybrid Quasi-solid Polymer Electrolyte based on Porous PVB and Modified PEG for Electrochromic Application," *Organic Electronics* 56 (2018): 268.
36. G. Malucelli, G. Gozzelino, F. Ferrero, R. Bongiovanni, and A. Priola, "Synthesis of Poly(propylene-glycol-diacrylates) and Properties of the Photocured Networks," *Journal of Applied Polymer Science* 65 (1997): 491.
37. J. Zeng, Z. Wan, M. Zhu, L. Ai, P. Liu, and W. Deng, "Flexible Electrochromic Energy-saving Windows with Fast Switching and Distability based on a Transparent Solid-state Electrolyte," *Materials Chemistry Frontiers* 3 (2019): 2514.
38. V. V. Krongauz, "Crosslink Density Dependence of Polymer Degradation Kinetics: Photocrosslinked Acrylates," *Thermochimica Acta* 503-504 (2010): 70.
39. T. Y. Lee, C. A. Guymon, E. S. Jönsson, and C. E. Hoyle, "The Effect of Monomer Structure on Oxygen Inhibition of (meth) Acrylates Photopolymerization," *Polymer* 45 (2004): 6155.
40. Y. Ding, M. Wang, Z. Mei, and X. Diao, "Different ion-based Electrolytes for Electrochromic Devices: A Review," *Solar Energy Materials and Solar Cells* 248 (2022): 112037.
41. T. Y. Yun, X. Li, J. Bae, S. H. Kim, and H. C. Moon, "Non-volatile, Li-doped ion gel Electrolytes for Flexible WO₃-based Electrochromic Devices," *Materials & Design* 162 (2019): 45.
42. A. R. Kannurpatti, J. W. Anseth, and C. N. Bowman, "A Study of the Evolution of Mechanical Properties and Structural Heterogeneity of Polymer Networks formed by Photopolymerizations of Multifunctional (meth)Acrylates," *Polymer* 39 (1998): 2507.
43. M. T. Otley, F. A. Alamer, Y. Zhu, et al., "Acrylated Poly(3,4-propylenedioxythiophene) for Enhancement of Lifetime and Optical Properties for Single-Layer Electrochromic Devices," *ACS Applied Materials & Interfaces* 6 (2014): 1734.
44. J. Reiter, O. Krejza, and M. Sedlaříková, "Electrochromic Devices Employing Methacrylate-based Polymer Electrolytes," *Solar Energy Materials and Solar Cells* 228 (2009): 167.
45. Y. L. Yap, A. H. You, and L. L. Teo, "Preparation and Characterization Studies of PMMA–PEO-blend Solid Polymer Electrolytes with SiO₂ filler and Plasticizer for Lithium ion Battery," *Ionics* 25 (2019): 3087.
46. P. Singh, A. Sachdeva, C. Bhargava, M. A. Alheety, and J. Sharma, "Electrical and Structural Properties of PEMA-Based Plasticized Polymer Electrolyte," *Macromolecular Symposia* 407 (2023): 2200107.

47. Deutsche Norm, Glas im Bauwesen, Bestimmung der lichttechnischen und strahlungsphysikalischen Kenngrößen von Verglasungen (Deutsches Institut für Normung, 2011).
48. C. Park, J. M. Kim, Y. Kim, et al., "High-Coloration Efficiency and Low-Power Consumption Electrochromic Film based on Multifunctional Conducting Polymer for Large Scale Smart Windows," *ACS Applied Electronic Materials* 3 (2021): 4781.
49. G. A. Giffin, A. Moretti, S. Jeong, and S. Passerini, "Decoupling Effective Li⁺ ion Conductivity from Electrolyte Viscosity for Improved Room-temperature Cell Performance," *Journal of Power Sources* 342 (2017): 335.
50. E. C. Constable and A. M. W. Cargill Thompson, "Multinucleating 2,2': 6',2''-Terpyridine Ligands as Building Blocks for the Assembly of Co-ordination Polymers and Oligomers," *Journal of the Chemical Society, Dalton Transactions* 24 (1992): 3467.
51. F. S. Han, M. Higuchi, and D. G. Kurth, "Diverse Synthesis of Novel Bisterpyridines via Suzuki-Type Cross-Coupling," *Organic Letters* 9 (2007): 559.
52. W. Cheng, M. Moreno-Gonzalez, K. Hu, et al., "Solution-Deposited Solid-State Electrochromic Windows," *iScience* 10 (2018): 80.
53. J. Zheng, W. Li, X. Liu, J. Zhang, X. Feng, and W. Chen, "Progress in Gel Polymer Electrolytes for Sodium-Ion Batteries," *Energy & Environmental Materials* 6 (2023): e12422.
54. O. Borodin, J. Self, K. A. Persson, C. Wang, and K. Xu, "Uncharted Waters: Super-concentrated Electrolytes," *Joule* 4 (2020): 69.
55. K. M. Diederichsen, H. G. Buss, and B. D. McCloskey, "The Compensation Effect in the Vogel-Tammann-Fulcher (VTF) Equation for Polymer-Based Electrolytes," *Macromolecules* 50 (2017): 3831.
56. N. Boaretto, Dissertation "Inorganic-organic Hybrid Polymer Electrolytes for Secondary Lithium Metal Batteries," (Università degli Studi di Padova, 2014).
57. F. Wang, F. Varenne, D. Ortiz, V. Pinzio, M. Mostafavi, and S. Le Caër, "Degradation of an Ethylene Carbonate/Diethyl Carbonate Mixture by Using Ionizing Radiation," *ChemPhysChem* 18 (2017): 2799.
58. S. Liang, W. Yan, X. Wu, et al., "Gel Polymer Electrolytes for Lithium ion Batteries: Fabrication, Characterization and Performance," *Solid State Ionics* 318 (2018): 2.
59. V. Bocharova and A. P. Sokolov, "Perspectives for Polymer Electrolytes: A View from Fundamentals of Ionic Conductivity," *Macromolecules* 11 (2020): 53.
60. H. Gu, C. Guo, S. Zhang, et al., "Highly Efficient, Near-Infrared and Visible Light Modulated Electrochromic Devices Based on Polyoxometalates and W₁₈O₄₉ Nanowires," *ACS Nano* 12 (2018): 559.
61. J. Padilla, L. Niklaus, M. Schott, et al., "Quantitative Assessment of the Cclng Stability of Different Electrochromic Materials and Devices," *ACS Applied Optical Materials* 1 (2023): 1174.
62. S. Hassab, D. E. Shen, A. M. Österholm, et al., "A New Standard Method to Calculate Electrochromic Switching Time," *Solar Energy Materials and Solar Cells* 185 (2018): 54.
63. E. Gileadi, *Physical Electrochemistry: Fundamentals, Techniques and Applications* (Wiley-VCH GmbH, 2011).
64. A. J. Bard, L. R. Faulkner, and H. S. White, *Electrochemical Methods: Fundamentals and Applications*, 3rd Edition, (John Wiley & Sons, Inc., 2001).
65. S. Halder, S. Garg, and C. Chakraborty, "Introducing Non-conjugated Ionic Spacer in Metallo-supramolecular Polymer: Generation of Nanofibers for High-performance Electrochromic Supercapacitor," *Chemical Engineering Journal* 470 (2023): 144361.
66. C. G. Granqvist, "Electrochromics for Smart Windows: Oxide-based Thin Films and Devices," *Thin Solid Films* 564 (2014): 1.
67. F. Wang, M. S. Wilson, R. D. Rauh, P. Schottland, B. C. Thompson, and J. R. Reynolds, "Electrochromic Linear and Star Branched Poly(3,4-ethylenedioxythiophene-didodecyloxybenzene) Polymers," *Macromolecules* 33 (2000): 2083.
68. K. M. Diederichsen, E. J. McShane, and B. D. McCloskey, "Promising Routes to a High Li⁺ Transference Number Electrolyte for Lithium Ion Batteries," *ACS Energy Letters* 2 (2017): 2563.
69. C. L. Gaupp, D. M. Welsh, R. D. Rauh, and J. R. Reynolds, "Composite Coloration Efficiency Measurements of Electrochromic Polymers Based on 3,4-Alkylenedioxythiophenes," *Chemistry of Materials* 14 (2002): 3964.
70. E. Barsoukov and J. R. Macdonald, *Impedance Spectroscopy: Theory, Experiment, and Applications*, (John Wiley & Sons, Inc., 2005).

Supporting Information

The authors have cited additional references within the Supporting Information. [47, 70, 68, 55, 69, 20]. Additional supporting information can be found online in the Supporting Information Section. **Supporting Fig. S1:** Normal force of GPE reference vs. GPE with PPGDA as a function of gap distance. **Supporting Fig. S2:** Transmittances of the Fe(II)-MCP/PB ECD with the GPE reference at 586 nm at the A) 5th and B) 1000th cycles as functions of time and the C) transmittance at 586 nm over 1000 cycles; t_{90} = response time. **Supporting Fig. S3:** Transmittances of the Fe(II)-MCP/PB ECD containing the GPE with PPGDA at 586 nm at the A) 5th and B) 1000th cycles as functions of time and the C) transmittance at 586 nm over 1000 cycles. **Supporting Fig. S4:** Time-dependent current and charge densities as functions of cycle number for bleaching and coloring of the Fe(II)-MCP/PB ECD with the GPE reference: Current densities of A) bleaching and B) coloring and charge densities of C) bleaching and D) coloring. **Supporting Fig. S5:** Time-dependent current and charge densities as functions of cycle number for bleaching and coloring of the Fe(II)-MCP/PB ECD containing the GPE with PPGDA: Current densities of A) bleaching and B) coloring and charge densities of C) bleaching and D) coloring. **Supporting Fig. S6:** Transmittances of the WO₃/NiO_x ECD with the GPE reference at 800 nm at the A) 5th and B) 1000th cycles as functions of time and the C) transmittance at 800 nm over 1000 cycles. **Supporting Fig. S7:** Transmittances of the WO₃/NiO_x ECD containing the GPE with PPGDA at 800 nm at the A) 5th and B) 1000th cycles as functions of time and the C) transmittance at 800 nm over 1000 cycles. **Supporting Fig. S8:** Time-dependent current and charge densities as functions of cycle number for bleaching and coloring of the WO₃/NiO_x ECD with the GPE reference: Current densities of A) bleaching and B) coloring and charge densities of C) bleaching and D) coloring. **Supporting Fig. S9:** Time-dependent current and charge densities as functions of cycle number for bleaching and coloring of the WO₃/NiO_x ECD containing the GPE with PPGDA: Current densities of A) bleaching and B) coloring and charge densities of C) bleaching and D) coloring. **Supporting Table S1:** CIE L*a*b* color coordinates of the Fe(II)-MCP/PB ECDs (4.0 cm × 3.5 cm) at cell voltages of 0.0/2.0 V (colored/bleached) and the WO₃/NiO_x ECDs (6.5 cm × 5.0 cm) at cell voltages of -1.7/1.0 V (colored/bleached).